# Effect of Al2O3/SiO2 on the structure and properties of blast furnace slag glass-ceramics

**Zuhao Li** ( 2677903458@qq.com )
Wuhan University of Technology
**Feng He**
Wuhan University of Technology
**Wentao Zhang**
Wuhan University of Technology
**Junlin Xie**
Wuhan University of Technology

**Research Article**

**Keywords:** glass-ceramics, blast furnace slag, Al2O3/SiO2, crystallization, sintering

**Posted Date:** December 22nd, 2020

**DOI:** https://doi.org/10.21203/rs.3.rs-131872/v1

# Abstract

Different $Al_2O_3/SiO_2$ glass-ceramics were prepared from blast furnace slag by traditional sintering method. The structure and properties of glasses or glass-ceramics were investigated by DSC, XRD, SEM, FTIR, $^{27}Al$ MAS NMR. The DSC results showed that with the increase of $Al_2O_3/SiO_2$, the glass transition temperature ($T_g$) first increased and then decreased, reached the minimum when $Al_2O_3/SiO_2$ was 0.34. The volume density, bending strength and microhardness of glass-ceramics also showed the same variation rule. The FTIR and $^{27}Al$ MAS NMR spectra results revealed this phenomenon. When $Al_2O_3/SiO_2$ was 0.19, a large amount of $Si^{4+}$ was added to the glass network to make the structure dense. With $Al_2O_3/SiO_2$ increased from 0.24 to 0.34, the amount of $[AlO_6]$ in the glass increased while $[AlO_4]$ decreased, and the degree of network polymerization of the glass decreased; as $Al_2O_3/SiO_2$ further increased from 0.34 to 0.39, $[AlO_4]$ increased and $[AlO_6]$ decreased in the glass, and the degree of network polymerization of the glass increased. The XRD results showed that the crystal phase of the glass-ceramics was composed of gehlenite, diopside and hyalophane. Moreover, with the increase of $Al_2O_3/SiO_2$, the gehlenite content in the glass-ceramics increased, while the content of diopside and hyalophane decreased.


# 1. Introduction

As a basic industry in China, steel industry produces about 200 billion tons of blast furnace slag (BFS)every year[1, 2]. Part of the BFS is directly used in low value-added products such as cement, slag brick and subgrade materials, however, a lot of BFS is dumped, which not only occupies land resources, but also causes serious pollution and waste[3]. In addition to some high titanium BFS, the main composition of BFS is CaO, MgO, $Al_2O_3$ and $SiO_2$, with the proportion of these four oxides exceeding 90 wt.%, which is similar to the composition of CMAS glass-ceramics, therefore, BFS is an excellent raw material for glass-ceramics[1, 3].

Glass-ceramics is a kind of polycrystalline solid material containing a large number of microcrystalline and glass phases, which is made by controlling crystallization of specific basic glass[4]. The special structure of glass-ceramics makes it have a variety of excellent properties, such as good insulation performance, high mechanical strength, low dielectric loss, etc.[5], which is a kind of products with high added value materials[4]. The preparation of glass-ceramics with BFS as raw material provides a new way for the recovery and utilization of BFS, which can alleviate the stacking and pollution of BFS and effectively improve the added value of the products.

In the composition of BFS, the content of $Al_2O_3$ and $SiO_2$ is more than 40 wt.%, in which $SiO_2$ acts as the glass network former, $Si^{4+}$ is connected in the shape of silicon-oxygen tetrahedron to form the basic network structure of glass. In the meantime, there are different degree of polymerization and depolymerization with different content of $SiO_2$ in glass, which is directly related to the heat treatment, termediate oxide, on the one hand, $Al^{3+}$ can

enter the glass network as [$AlO_4$], making the structure compact; on the other hand, $Al^{3+}$ can also exist in the glass as [$AlO_6$], causing the depolymerization of the glass network and making the structure loose[7]. In partial systems, $Al^{3+}$ can also act as the element of partial crystal phases when the content of $Al_2O_3$ is high[8]. Wentao Zhang et al. studied the influence of $B_2O_3/Al_2O_3$ ratio and Al/Na ratio on BFS glass-ceramics, and indicated that $Al_2O_3$ improved the thermal stability of glass, meanwhile, the crystallization activation energy and network structure were also affected with the change of $Al_2O_3$ content[9, 10]. Lishun Chen et al. also confirmed that, in the study of glass-ceramics with high calcium system, the crystallization activation energy rose and the main crystal phase changed from akermanite to gehlenite with the increase of $Al_2O_3$[11]. Jinshu Cheng et al. showed that the workability and kinetic fragility of glass were linked with the structure, with the increase of $SiO_2/Al_2O_3$, the non-bridging oxygen in the glass network decreased, and the structure of the glass network became compact, resulting in the increase of the viscosity of the glass melt, meanwhile, the change of $SiO_2/Al_2O_3$ ratio were responsible for the increase of fragility[12]. The research of Janusz Partyka et al. also showed that the variation of $SiO_2/Al_2O_3$ ratio directly determined the type and content of crystal phase[13]. Therefore, it is important to investigate the influence of $SiO_2/Al_2O_3$ on the structure and properties of BFS glass-ceramics.

In this paper, based on 60 wt.% BFS, the effects of different $SiO_2/Al_2O_3$ on the crystal phases, structure and properties of glass-ceramics were studied. In order to further reveal the influence of the $Al_2O_3/SiO_2$ on the glass network, Fourier Transform Infrared Spectrometer and Solid State Nuclear Magnetic Resonance Spectrometer were used to deeply investigate the microstructure of glass and glass-ceramics.

## 2. Experiment

# 2.1 Raw materials and experimental formula

The BFS used in this experiment was from China Baowu Iron & Steel Group. The chemical composition of BFS was measured by X-ray Fluorescence (XRF, Zetium, PANalytical B. V.). This experiment was based on 60 wt.% BFS and supplemented by pure chemical reagent to prepare glass-ceramics. The high content of alkaline earth metal oxide in BFS leads to the high alkalinity of base glass, which is not conducive to the sintering process due to the fast crystallization[14]. Therefore, the reagents were mainly acid oxides such as $SiO_2$ and $Al_2O_3$, and a small amount of oxides such as $Na_2O$, $K_2O$, BaO and $B_2O_3$ were added to adjust the glass melting, clarification, homogenization and sintering process. The oxides were introduced by $Na_2CO_3$, $K_2CO_3$, $Ba_2CO_3$ and $H_3BO_3$ respectively. The formula and the specific oxide composition of the BFS were shown in Table 1. The $SiO_2/Al_2O_3$ ratios in the base glass were different, which were 0.19(A1), 0.24(A2), 0.29(A3), 0.34(A4) and 0.39(A5), respectively.

Table 1

Oxide composition of glasses and BFS (wt.%).

| | $Al_2O_3$ | $SiO_2$ | CaO | MgO | BaO | $Na_2O$ | $K_2O$ | $B_2O_3$ | others | Al/Si |
|---|---|---|---|---|---|---|---|---|---|---|
| BFS | 15.12 | 31.92 | 39.81 | 8.54 | 0.12 | 0.39 | 0.58 | / | 3.52 | 0.47 |
| A1 | 9.07 | 48.19 | 23.89 | 5.12 | 3.00 | 3.00 | 3.00 | 2.00 | 2.73 | 0.19 |
| A2 | 11.08 | 46.18 | 23.89 | 5.12 | 3.00 | 3.00 | 3.00 | 2.00 | 2.73 | 0.24 |
| A3 | 12.87 | 44.39 | 23.89 | 5.12 | 3.00 | 3.00 | 3.00 | 2.00 | 2.73 | 0.29 |
| A4 | 14.53 | 42.73 | 23.89 | 5.12 | 3.00 | 3.00 | 3.00 | 2.00 | 2.73 | 0.34 |
| A5 | 16.07 | 41.19 | 23.89 | 5.12 | 3.00 | 3.00 | 3.00 | 2.00 | 2.73 | 0.39 |

## 2.2 Preparation of glass-ceramics

In this paper, glass-ceramics were prepared using conventional sintering method. The melting temperature of the base glass was 1450 ℃, the holding time was 1 h. The melted glass liquid was poured into the clear water to obtain the base glass slag. And the glass slag was ground with planetary grinding ball for 30 min and then passed through a 200 mesh sieve to obtain the parent glass powder which was pressed into 4 mm × 40 mm strip samples under a pressure of 50 MPa, and then the samples were sintered in a resistance furnace, the sintering temperature was obtained by thermal analysis, the heating rate was 10 ℃/min, the holding time was 1.5 h.

## 2.3 Characterizations

Thermal analysis of base glass powder was performed using Differential Scanning Calorimetry (DSC, STA449F3, NETZSCH), the temperature range was 0-1000 ℃ in the air and the heating rate was 10 ℃/min. The crystal phase was measured by X-ray Diffractometer (XRD, D8 Advance, BRUKER AXS),the scanning range was 10–70º.The micromorphology of the glass-ceramics was observed by Field Emission Scanning Electron Microscope (FESEM, Zeiss Ultra Plus, Zeiss Germany), the polished surface was etched with HF solution (4%) for 40 s. The microstructure of both glasses and glass-ceramics was measured by Fourier Transform Infrared Spectrometer (FTIR, Nexus, Thermo Nicolet) at range of 400–2000 $cm^{-1}$. The $^{27}Al$ NMR spectra of the base glasses were measured by Solid State Nuclear Magnetic Resonance Spectrometer (NMR, AVANCE Ⅲ).

The bending strength (M, MPa) of glass-ceramics was measured by three-point test method, and the calculation formula was as follows:

$$M = \frac{3FL}{2bh^2}$$

where *F* is the fracture load (N), *L* is the span (mm), *b* is the fracture width (mm), and *h* is the fracture thickness (mm). The volume density of glass-ceramics was measured by Archimedes-drainage method. The indentation method was used to measure the Vickers hardness of the glass-ceramics, the loading

# 3. Results And Discussion

# 3.1 DSC analysis

Figure 1 showed the DSC graph of parent glasses with different $Al_2O_3/SiO_2$ at heating rate of 10 ℃/min. Table 2 showed the specific characteristic temperature values for A1-A5, where $T_g$ was the glass transition temperature, $T_{c1}$ was the first crystallization temperature, and $T_{c2}$ was the second crystallization temperature. In Fig. 1, there were two obvious exothermic peaks within the range of 780–900 ℃, among which the first crystal peak shape of A1 parent glass was relatively flat.

Table 2

Characteristic temperature of glasses with different $Al_2O_3/SiO_2$ in DSC.

| | $T_g$(℃) | $T_{c1}$(℃) | $T_{c2}$(℃) |
|---|---|---|---|
| A1 | 613.7 | 851.8 | 900.8 |
| A2 | 594.7 | 799.0 | 878.8 |
| A3 | 568.8 | 790.8 | 887.1 |
| A4 | 413.1 | 783.7 | 886.2 |
| A5 | 565.2 | 783.5 | 886.0 |

The DSC curve of the base glasses showed that the peak of $T_{c1}$ became sharp and moved towards low temperature gradually for A1-A5, while $T_{c2}$ showed a trend of moving towards high temperature for A2-A5. While the charge of $Al^{3+}$ is less than that of $Si^{4+}$, and the self-diffusion coefficient of $Al^{3+}$ is higher than that of $Si^{4+}$[15]. Therefore, the higher $Al_2O_3$ content in the glasses was more conducive to particle diffusion in the crystallization process, which reduced $T_{c1}$ for A1-A5[15]; then the crystal phase was precipitated on the surface of the glass particle, which increased the viscosity of the glasses, hindered the further diffusion of the particle, and led to the rise of $T_{c2}$[16]. The first crystallization peak of the A1 glass was not obvious and the $T_{c2}$ was high, which may be related to the high $SiO_2$ content in the A1 glass, as $Si^{4+}$ can gather the network, increase the viscosity of the glass, hinder the diffusion of particles inside the glass, and increase the crystallization temperature[17]. Figure 1 and Table 2 showed that $T_g$ decreased first from A1 to A5 (reached the minimum in A4) and then increased, which indicated that the thermal stability of glasses deduced first and then rose with the increase of $Al_2O_3/SiO_2$. The thermal stability of glasses is closely related to the network structure of glass[18], which also indicated that the network polymerization degree of glasses showed a trend of first decreasing and then increasing in series A glasses. In this experiment, according to the DSC curve (Fig. 1), in order to ensure that the crystallization process of each sample was fully carried out, the sintering temperature of the sample was set at 890 ℃ and the holding time was 1.5 h.

# 3.2 Crystal phase analysis

The XRD graph of glass-ceramics with different $Al_2O_3/SiO_2$ was illustrated in Fig. 2. It shows that the peaks of A1-A5 glass-ceramics were basically the same. The analysis by Jade 6.5 indicated that the crystal phase of A series glass-ceramics was composed of the main crystal phase gehlenite($Ca_2(Al(AlSi)O_7$,PDF#74-1607), the secondary crystal phase diopside($CaMgSi_2O_6$PDF#74-1607) and hyalophane ($K._6Ba._4Al_{1.42}Si_{2.58}O_8$PDF#72-1497). Figure 2 also showed that the diffraction peak intensity of the main crystal phase increased while that of the secondary crystal phase decreased gradually for A1-A5.

It means that the content of gehlenite in the glass-ceramics increased while diopside and hyalophane decreased with the increase of $Al_2O_3/SiO_2$. The degree of polymerization of anionic groups is different between the primary phase (gehlenite) and the secondary phase (diopside and hyalophane). The reaction process is as follows:

$$2Ca^{2+} + Al^{3+} + (AlSiO_7)^{7-} \rightarrow Ca_2Al(AlSi)O_7$$

$$Ca^{2+} + Mg^{2+} + (Si_2O_6)^{4-} \rightarrow CaMgSi_2O_6$$

$$0.6K^{+} + 0.4Ba^{2+} + (Al_{1.42}Si_{2.58}O_8)^{1.42-} \rightarrow K._6Ba._4Al_{1.42}Si_{2.58}O_8$$

The Si(Al)/O ratio of anion group $[AlSiO_7]$ is smaller than that of $[Si_2O_6]$ and $[Al_{1.42}Si_{2.58}O_8]$, indicating a lower degree of polymerization of $[AlSiO_7]$[19, 20]. In terms of element composition, $Al^{3+}$ directly participated in the formation of the main crystal phase gehlenite, therefore, the increase of $Al_2O_3$ content was conducive to the precipitation of gehlenite. As a network intermediate, $Al^{3+}$ can not only replace $Si^{4+}$ to participate in the glass network and crystal phase constitution with $[AlO_4]$, but also destroy the glass network structure in the form of $[AlO_6]$[7, 8]. On the one hand, with the increase of $Al_2O_3/SiO_2$, $Si^{4+}$ in the glass decreased and $Al^{3+}$ increased, $[AlO_6]$ played a role in breaking the glass network, reducing the degree of polymerization of glass network and facilitating the precipitation of gehlenite with low degree of anionic polymerization; on the other hand, the increase of $Al_2O_3$ rose the number of $Al^{3+}$ substituted for $Si^{4+}$ in the glass network, which was conducive to the formation of $[AlSiO_7]$ and promoted the precipitation of gehlenite. On account of the large amount of precipitation of gehlenite, $Si^{4+}$ content in the glasses was decreased, which led to the reduction of the anion group of the secondary crystal phase and reduced the precipitation of diopside and hyalophane.

The SEM graph was showed in Fig. 3. It illustrated that there were a large number of strip or gridded crystals, and the XRD analysis results showed that the crystal phase was gehlenite; a few clusters of granular crystals were seen in A1-A3, which were speculated to be diopside based on the XRD results. In the A4 and A5 samples, no other crystal phases were found, which was mainly attributed to the high ondary phase. In the SEM graph of A1, there

were more holes left by HF solution erosion. With the increase of $Al_2O_3/SiO_2$, the holes decreased gradually, indicating that the increase of crystal evolution led to the decrease of glass phase for A1-A5. When the $Al_2O_3/SiO_2$ increased to 0.34 (A4), it was seen that the growth of crystal grains was united and arranged in a certain direction, and the defect area without crystal phase existed; when the $Al_2O_3/SiO_2$ ratio continued to increase to 0.39 (A5), the crystal grains continued to grow into long strips, and the long strips growing in different directions were interspersed and nested together.

# 3.3 FTIR analysis

FTIR is a common method used to test the internal structure of glass and glass-ceramics. Figure 4 was the FTIR of the base glasses with different $Al_2O_3/SiO_2$ at 400 $cm^{-1}$-1400 $cm^{-1}$. In Fig. 4, the shape of vibration absorption peak of A1-A5 parent glasses was substantially the same. There were mainly three wide vibration absorption bands, which were in the range of 400–600 $cm^{-1}$, 600–800 $cm^{-1}$ and 800–1200 $cm^{-1}$ respectively. The irregular arrangement of ions (ion clusters) in the glasses and the existence of non-bridging oxygen bonds made the angle and length of Si-O bond change, which made the infrared vibration absorption peak shift to a certain extent and become gentle and broad[21, 22].

In the infrared vibration spectra of glasses, the vibration absorption band in the range of 400–600 $cm^{-1}$ was attributed to the bending vibration of Si–O–Si, Si–O–Al, O–Si–O and O–Al–O[23, 24].

The absorption peak in the range of 600–800 $cm^{-1}$ was the symmetric stretching vibration of Si–O–Al, which was mainly attributed to the stretching vibration of the [$AlO_4$] and stretching vibration of the bridge oxygen bond in the glass network structure[11]. From A1 to A5, the vibration absorption peak near 720 $cm^{-1}$ showed a small shift towards low wavenumbers, and the absorption intensity was enhanced, indicating that the Si–O–Al bond with lower vibration frequency in the glass network increased[23]. This was due to the fact that with the increase of $Al_2O_3/SiO_2$, more and more $Al^{3+}$ replaced $Si^{4+}$ to form tetrahedron and entered into the glass network, forming Si–O–Al bond with [$SiO_4$].

The absorption vibration peak in the range of 800–1200 $cm^{-1}$ was mainly related to the [$SiO_4$], which was attributed to the asymmetric stretching vibration of Si–O–Si, the symmetric stretching vibration and asymmetric stretching vibration of O–Si–O, the absorption was strong and broad, which was caused by the superposition of different peaks[25–27]. The vibration absorption peak in the range of 800–1200 $cm^{-1}$ can be decomposed into stretching vibration of silicon-oxygen tetrahedron with different degree of polymerization by Gaussian function (Fig. 5), whose symbol is $Q^n$, where n is the number of bridging oxygen ($O_b$) in the silicon-oxygen tetrahedron (n = 0,1,2,3,4,5)[19, 28]. Figure 5 was the Gaussian deconvolution diagram of the infrared vibration absorption peak at the range of 800–1200 $cm^{-1}$ of the series A glasses, and table 3 was the specific peak values of each $Q^n$. The results of Fig. 5 and Table 3 showed that the vibration absorption peaks of A1-A5 glasses at 800–1200 $cm^{-1}$ were all decomposed into 5 vibration absorption peaks corresponding to $Q^0$, $Q^1$, $Q^2$, $Q^3$ and $Q^4$ respectively. Moreover, the peak

positions of $Q^n$ were relatively similar for each sample of series A glasses, indicating that the network structure of the base glass did not change significantly with the increase of $Al_2O_3/SiO_2$.

Figure 6 was the variation distribution chart of peak position of $Q^n$ for A1-A5, which indicated that the peak position of $Q^n$ was firstly shifted to direction of the low wavenumbers and then to the high wavenumbers, among which the peak position of $Q^n$ reached the lowest when the $Al_2O_3/SiO_2$ was 0.34 (A4). The vibration absorption peak of $Q^n$ is closely related to the glass network[29]. When the glass network tends to be close, the vibration peak is shifted to the direction of high wavenumbers; on the contrary, when the glass network structure tends to be loose, the vibration peak moves to the direction of low wavenumbers[29]. The curve in Fig. 6 illustrated that the glass network structure tended to be loose with the increase of $Al_2O_3/SiO_2$ from 0.19 to 0.34; subsequently, the glass network structure tended to be close with the $Al_2O_3/SiO_2$ continues to increase from 0.34 to 0.39.

Table 3

Wavenumbers of $Q^n$ in glasses with different $Al_2O_3/SiO_2$.

| | | A1 | A2 | A3 | A4 | A5 |
|---|---|---|---|---|---|---|
| Wavenumbers ($cm^{-1}$) | $Q^0$ | 849.7 | 847.2 | 847.1 | 844.1 | 844.1 |
| | $Q^1$ | 894.6 | 890.6 | 889.0 | 883.5 | 886.2 |
| | $Q^2$ | 970.2 | 962.4 | 956.6 | 948.4 | 959.6 |
| | $Q^3$ | 1069.5 | 1061.6 | 1054.5 | 1049.2 | 1060.9 |
| | $Q^4$ | 1144.7 | 1140.1 | 1136.5 | 1132.2 | 1135.9 |

The infrared vibration absorption spectra of the glass-ceramics sintered at 890 °C was showed in Fig. 7. It indicated that the peak range of the glass-ceramics sample was roughly the same as that of the base glasses (Fig. 4), which was still divided into three vibration absorption bands, however, there were some sharp absorption peaks which were not found in the infrared vibration absorption spectra of the base glasses. This was mainly attributed to the generation of crystal phase, which made the originally covered absorption peaks appear[21, 23]. The position and shape of the infrared absorption peaks of A1-A5 were basically the same, indicating that the crystal phase of glass-ceramics with different $Al_2O_{3/}SiO_2$ were basically the same, and the XRD analysis also proves this conclusion.

In the range of 400-600$cm^{-1}$, the vibration absorption peak at 470 $cm^{-1}$ was divided into two absorption peaks: 472 $cm^{-1}$ and 424 $cm^{-1}$. The peak at 472 $cm^{-1}$ was attributed to the bending vibration of Si–O–Si in the residual glass phase and diopside phase (a small amount of hyalophane), the peak at 424 $cm^{-1}$ [illegible] gehlenite[24, 30]. The intensity of the vibration

absorption peak at 424 $cm^{-1}$ gradually increased for A1-A5, which indicated that the content of gehlenite increased in glass ceramics with the increase of $Al_2O_3/SiO_2$. There were two vibration absorption peaks at 544 $cm^{-1}$ and 579 $cm^{-1}$, which were not found in the base glasses in Fig. 4. This was due to the coupling effect between the bending vibration of O-Si-O in the crystal phase and the stretching vibration of Ca–O[24, 27]. In the range of 600–800 $cm^{-1}$, in addition to the vibration absorption peak near 714 $cm^{-1}$(base glasses also had the same vibration absorption peak), two new vibration absorption peaks appeared at 682 $cm^{-1}$ and 630 $cm^{-1}$. The peak at 714 $cm^{-1}$ and 682 $cm^{-1}$ were attributed to the symmetric stretching vibration of Si–O–Si and the stretching vibration of Si–O–Al respectively; the peak at 630 $cm^{-1}$ was related to the stretching vibration of Al–O in the aluminum-oxygen tetrahedron[22, 27, 30]. In the range of 800–1200 $cm^{-1}$, the vibration absorption peak near 1000 $cm^{-1}$ split into 1028 $cm^{-1}$, 985 $cm^{-1}$ and 939 $cm^{-1}$ due to crystal phase precipitation, which were associated with the stretching vibration of Si–O in [$SiO_4$] (asymmetric stretching vibration of Si–O–Si, symmetric stretching vibration and asymmetric stretching vibration of O–Si–O)[22, 26, 27].

## 3.4 $^{27}$Al NMR analysis

To further study the coordination of $Al^{3+}$ in glass, the $^{27}$Al MAS NMR spectra were used to investigate the glass structure, as shown in Fig. 8, there was an obvious wide peak in the range of -25-100 ppm. In aluminosilicate system, $Al^{3+}$ has three coordination modes: [$AlO_4$], [$AlO_5$], [$AlO_6$]. Therefore[31, 32], $^{27}$Al NMR spectra were deconvoluted by Gaussian function, and the results were shown in Fig. 9 and Fig. 10.

The results in Fig. 9 showed that the $^{27}$Al NMR spectra deconvolution of series A glasses were similar, which was consisted of three distinct peaks [$AlO_4$], [$AlO_5$] and [$AlO_6$], in which the area % of [$AlO_n$] (n = 4, 5, 6) was related to its content[7, 9, 10]. In Fig. 10, the area % of [$AlO_6$] first increased and then decreased for A2-A5, and reached the maximum in A4 (the $Al_2O_3/SiO_2$ was 0.34); on the contrary, the area % of [$AlO_5$] and [$AlO_4$] first decreased and then increased, and reached the minimum in A4. The area % of [$AlO_6$] in A1 glass was relatively large, while area % of [$AlO_5$] and [$AlO_4$] were relatively small, which may be related to the small $Al_2O_3/SiO_2$ in A1. The high $SiO_2$ content in the glass made the glass network densified, at the same time, the low $Al_2O_3$ content made it difficult for $Al^{3+}$ to replace $Si^{4+}$ in glass network, hence, more $Al^{3+}$ existed in [$AlO_6$] for A1.

## 3.5 Physical and mechanical properties analysis

The physical and mechanical properties of glass-ceramics with different $Al_2O_3/SiO_2$ were showed in Fig. 11; (a), (b) and (c) were the volume density, the bending strength and the microhardness respectively.

The results of Fig. 8 showed that the volume density of the glass-ceramics was between 2.735–2.770 g/$cm^3$, the bending strength was between 95–120 MPa and the microhardness was between 540–610 Hv. Meanwhile, with the increase of $Al_2O_3/SiO_2$, the volume density, bending strength and microhardness of glass-ceramics all decreased first (reached the minimum in A4, the $Al_2O_3/SiO_2$ was

0.34) and then increased. The physical and mechanical properties of glass-ceramics are closely connected to the crystal phase, the glass phase and the combination among them[33, 34]. According to the previous analysis, with the $Al_2O_3/SiO_2$ gradually raising from 0.19 to 0.34, the precipitation of main crystal phase gehlenite ($Ca_2(Al(AlSi)O_7)$) increased, while the precipitation of secondary crystal phase decreased, and the remaining glass phase in the glass-ceramics also decreased. With the precipitation and growth of crystal phase, the internal stress of the glass-ceramics rose, and the decrease of liquid phase content was harmful to the sintering process, which led to the insufficient connection between crystal phase and led to more holes and defects in the glass-ceramics. At the same time, more $Al^{3+}$ destroyed the glass network structure with $[AlO_6]$, making the microstructure of the glasses tend to be loose. These results combined to reduce the physical properties (volume density, bending strength, microhardness) of the glass-ceramics with the increase of $Al_2O_3/SiO_2$ from 0.19–0.34 (A1-A4). With the further increase of $Al_2O_3/SiO_2$ from 0.34 to 0.39, the proportion of $[AlO_4]$ in the glass network increased, which was beneficial to strengthen the glass network and make the structure tend to be dense. Meanwhile, the crystal phase in the glass-ceramics was further precipitated and grown, and the long strip crystal phase was interspersed with each other, which made the bonding between the crystal phase more complex and compact, thus increasing the density, bending strength and microhardness.

# 4. Conclusion

The effects of different $Al_2O_3/SiO_2$ on the structure and properties of BFS glass-ceramics were studied in this paper. With the increase of $Al_2O_3/SiO_2$, the gehlenite content in the glass-ceramics increased, while the diopside and hyalophane contents decreased. As $Al_2O_3/SiO_2$ increased from 0.24 to 0.34, the content of $[AlO_6]$ in the glass network increased and $[AlO_4]$ decreased gradually, the glass network structure became loose and the temperature of $T_g$ decreased, simultaneously, the volume density, bending strength and microhardness of the glass-ceramics also decreased. With further increased $Al_2O_3/SiO_2$ from 0.34 to 0.39, the content of $[AlO_6]$ in the glass decreased and $[AlO_4]$ increased, the glass network structure became densified and the temperature of $T_g$ increased, meanwhile, the volume density, bending strength and microhardness of the glass-ceramics increased. When $Al_2O_3/SiO_2$ was 0.19, the network structure of glass was relatively compact as high $SiO_2$ content, and the performance of glass-ceramics was the best, the volume density was 2.77 $g/cm^3$, the bending strength was 120.50 MPa, the microhardness was 604.21 Hv.

# Declarations


# Acknowledgement

We acknowledge Dr. Yumei Li (Center for Material research and analysis, Wuhan University of Technology, China) for the FESEM analyses.

# References


1. Jia RD, Deng LB, Yun F, Li H, Zhang XF, Jia XL (2019) Effects of $SiO_2$/CaO ratio on viscosity, structure, and mechanical properties of blast furnace slag glass ceramics. Mater Chem Phys 233:155–162
2. He T, Li Z, Zhao S, Zhao X, Qu X, Study on the particle morphology, powder characteristics and hydration activity of blast furnace slag prepared by different grinding methods, Construction and Building Materials, (2020) 121445
3. Oge M, Ozkan D, Celik MB, Gok MS, Karaoglanli AC, An Overview of Utilization of Blast Furnace and Steelmaking Slag in Various Applications, Mater. Today-Proc., 11 (2019) 516–525
4. Deng BH, Luo J, Harris JT, Smith CM, McKenzie ME (2019) Molecular dynamics simulations on fracture toughness of $Al_2O_3$-$SiO_2$ glass-ceramics. Scr Mater 162:277–280
5. Dechandt ICJ, Soares P, Pascual MJ, Serbena FC (2020) Sinterability and mechanical properties of glass-ceramics in the system $SiO_2$-$Al_2O_3$-MgO/ZnO. J. Eur Ceram Soc 40:6002–6013
6. Diallo B, Allix M, Veron E, Sarou-Kanian V, Bardez-Giboire I, Montouillout V, Pellerin N (2019) Deconvolution method of $^{29}$Si MAS NMR spectra applied to homogeneous and phase separated lanthanum aluminosilicate glasses. J Non-Cryst Solids 503:352–365
7. Novikov AN, Neuville DR, Hennet L, Gueguen Y, Thiaudiere D, Charpentier T, Florian P (2017) Al and Sr environment in tectosilicate glasses and melts: Viscosity, Raman and NMR investigation. Chem Geol 461:115–127
8. Kwinda TI, Koppka S, Sander SAH, Kohns R, Enke D (2020) Effect of $Al_2O_3$ on phase separation and microstructure of $R_2O$-$B_2O_3$-$Al_2O_3$-$SiO_2$ glass system (R = Li, Na). J Non-Cryst Solids 531:119849
9. Zhang WT, He F, Xiao YL, Xie MQ, Xie JL, Sun RJ, Yang H, Luo ZH (2019) Effects of Al/Na and heat treatment on the structure and properties of glass ceramics from molten blast furnace slag. Ceram Int 45:13692–13700
10. Zhang WT, He F, Xiao YL, Xie MQ, Xie JL, Li FX, Yang H, Li ZH (2020) Structure, crystallization mechanism, and properties of glass ceramics from molten blast furnace slag with different $B_2O_3$/$Al_2O_3$. Mater Chem Phys 243:122664
11. Chen LS, Ge XX, Long YT, Zhou MK, Wang HD, Chen X (2020) Crystallization and properties of high calcium glass-ceramics synthesized from ferromanganese slag. J Non-Cryst Solids 532:119864
12. Cheng JS, Xiao ZF, Yang K, Wu H (2013) Viscosity, fragility and structure of $Na_2O$-CaO-$Al_2O_3$-$SiO_2$ glasses of increasing Al/Si ratio. Ceram Int 39:4055–4062
13. Partyka J, Leśniak M (2016) Raman and infrared spectroscopy study on structure and microstructure of glass–ceramic materials from $SiO_2$-$Al_2O_3$-$Na_2O$-$K_2O$-CaO system modified by variable molar ratio of $SiO_2$/$Al_2O_3$. Spectrochim Acta Part A Mol Biomol Spectrosc 152:82–91
14. Zeng L, Sun HJ, Peng TJ, Zheng WM (2019) The sintering kinetics and properties of sintered glass-ceramics from coal fly ash of different particle size. Results Phys 15:102774

15. Jiang CH, Li KJ, Zhang JL, Qin QH, Liu ZJ, Sun MM, Wang ZM, Liang W (2018) Effect of $MgO/Al_2O_3$ ratio on the structure and properties of blast furnace slags: A molecular dynamics simulation. J Non-Cryst Solids 502:76–82
16. Karamanov A, Hamzawy EMA, Karamanova E, Jordanov NB, Darwish H (2020) Sintered glass-ceramics and foams by metallurgical slag with addition of $CaF_2$. Ceram Int 46:6507–6516
17. Li B, Li W, Zheng J (2017) Effect of $SiO_2$ content on the sintering kinetics, microstructures and properties of $BaO\text{-}Al_2O_3\text{-}B_2O_3\text{-}SiO_2$ glass-ceramics for LTCC application. J Alloy Compd 725:1091–1097
18. Zhang WT, He F, Xie JL, Liu XQ, Fang D, Yang H, Luo ZH (2018) Crystallization mechanism and properties of glass ceramics from modified molten blast furnace slag. J Non-Cryst Solids 502:164–171
19. Deng LB, Jia RD, Yun F, Zhang XF, Li H, Zhang MX, Jia XL, Ren D, Li BW (2020) Influence of $Cr_2O_3$ on the viscosity and crystallization behavior of glass ceramics based on blast furnace slag. Mater Chem Phys 240:122212
20. Akatov AA, Nikonov BS, Omel'yanenko BI, Stefanovsky SV, Marra JC (2009) Structure of borosilicate glassy materials with high concentrations of sodium, iron, and aluminum oxides. Glass Phys Chem 35:245–259
21. Ma M, Ni W, Wang Y, Wang Z, Liu F (2008) The effect of $TiO_2$ on phase separation and crystallization of glass-ceramics in $CaO\text{-}MgO\text{-}Al_2O_3\text{-}SiO_2\text{-}Na_2O$ system. J Non-Cryst Solids 354:5395–5401
22. Deng LB, Yun F, Jia RD, Li H, Jia XL, Shi Y, Zhang XF (2020) Effect of $SiO_2/MgO$ ratio on the crystallization behavior, structure, and properties of wollastonite-augite glass-ceramics derived from stainless steel slag. Mater Chem Phys 239:122039
23. Shi J, He F, Ye CQ, Hu L, Xie JL, Yang H, Liu XQ (2017) Preparation and characterization of $CaO\text{-}Al_2O_3\text{-}SiO_2$ glass-ceramics from molybdenum tailings. Mater Chem Phys 197:57–64
24. Luo W, Bao ZH, Jiang WH, Liu JM, Feng G, Xu YQ, Tang HD, Wang T (2019) Effect of $B_2O_3$ on the crystallization, structure and properties of $MgO\text{-}Al_2O_3\text{-}SiO_2$ glass-ceramics. Ceram Int 45:24750–24756
25. Kim ES, Yeo WJ (2012) Thermal properties of $CaMgSi_2O_6$ glass–ceramics with $Al_2O_3$. Ceram Int 38:S547–S550
26. Ghosh TK, Mukherjee DP, Ghorai UK, Das SK, Synthesis and crystallisation kinetics study of nano-$Al_2O_3$ containing bio-active glass-ceramics, Mater. Today-Proc., 11 (2019) 794–803
27. Montoya-Quesada E, Villaquiran-Caiced MA, de Gutierrez RM, Munoz-Saldana J (2020) Effect of ZnO content on the physical, mechanical and chemical properties of glass-ceramics in the $CaO\text{-}SiO_2\text{-}Al_2O_3$ system. Ceram Int 46:4322–4328
28. Zhao MZ, Cao JW, Wang Z, Li GH (2019) Insight into the dual effect of $Fe_2O_3$ addition on the crystallization of $CaO\text{-}MgO\text{-}Al_2O_3\text{-}SiO_2$ glass-ceramics. J Non-Cryst Solids 513:144–151

29. Chen MT, He F, Shi J, Xie JL, Yang H, Wan P (2019) Low $Li_2O$ content study in $Li_2O$-$Al_2O_3$-$SiO_2$ glass-ceramics. J Eur Ceram Soc 39:4988–4995
30. Pei FJ, Guo HW, Li P, Yan BJ, Li J, Yang P, Zhu GH (2018) Influence of low magnesia content on the CaO-$Al_2O_3$-$SiO_2$ glass-ceramics: Its crystallization behaviour, microstructure and physical properties. Ceram Int 44:20132–20139
31. Wilson PT, Chahal S, Pumlianmunga MM, Kumar K (2019) Ramesh, $^{27}$Al MAS NMR investigations on $Al_{23}Te_{77}$ glass: Observation of 5-coordinated Al and its influence on electrical switching. Solid State Commun 293:53–57
32. Kusumoto H, Hill RG, Karpukhina N, Law RV (2019) Magnesium substitution in calcium and strontium fluoro-phospho-aluminosilicate glasses by multinuclear $^{19}$F, $^{31}$P, $^{27}$Al, and $^{29}$Si MAS-NMR spectroscopy. Journal of Non-Crystalline Solids: X 1:100008
33. Inage K, Akatsuka K, Iwasaki K, Nakanishi T, Maeda K, Yasumori A (2020) Effect of crystallinity and microstructure on mechanical properties of CaO-$Al_2O_3$-$SiO_2$ glass toughened by precipitation of hexagonal $CaAl_2Si_2O_8$ crystals. J Non-Cryst Solids 534:119948
34. Gui H, Lin CW, Zhang Q, Luo ZW, Han L, Liu JL, Liu TY, Lu AX (2019) Glass forming, crystallization, and physical properties of MgO-A1$_2O_3$-$SiO_2$-$B_2O_3$ glass-ceramics modified by ZnO replacing MgO. J Eur Ceram Soc 39:1397–1410

# Figures

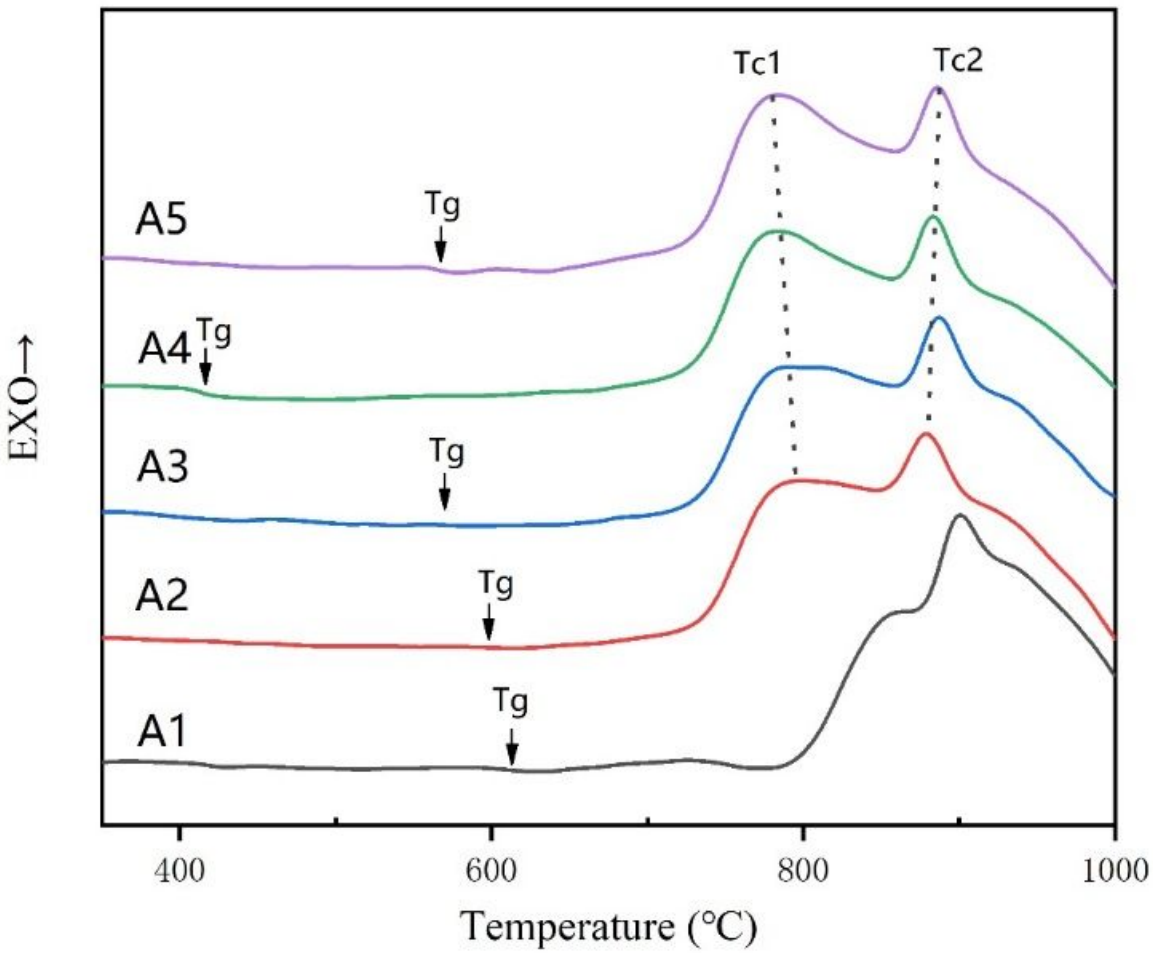


**Figure 1**

DSC of glasses with different Al2O3/SiO2 at 10 °C/min.

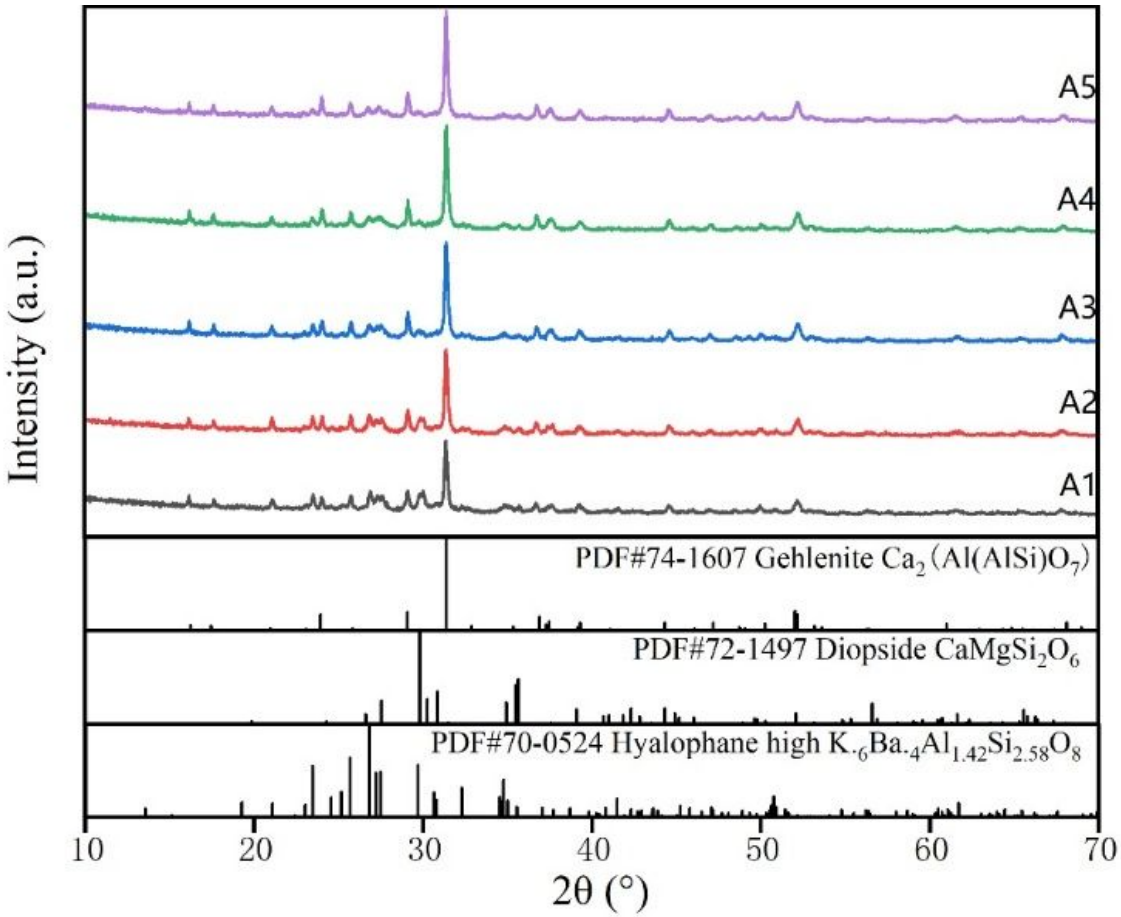


## Figure 2

XRD of glass-ceramics with different Al2O3/SiO2.

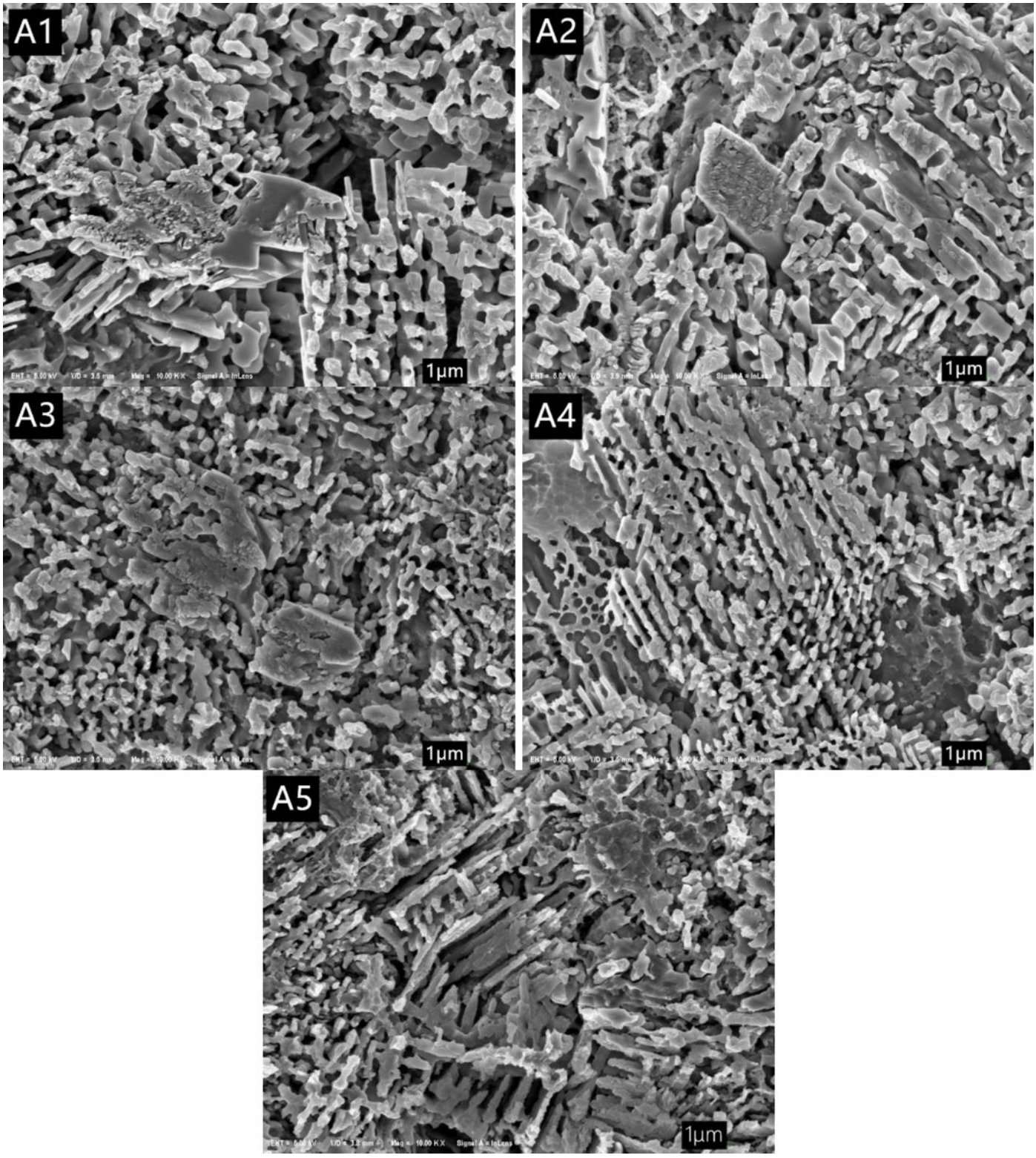


## Figure 3

SEM of glass-ceramics with different Al2O3/SiO2.

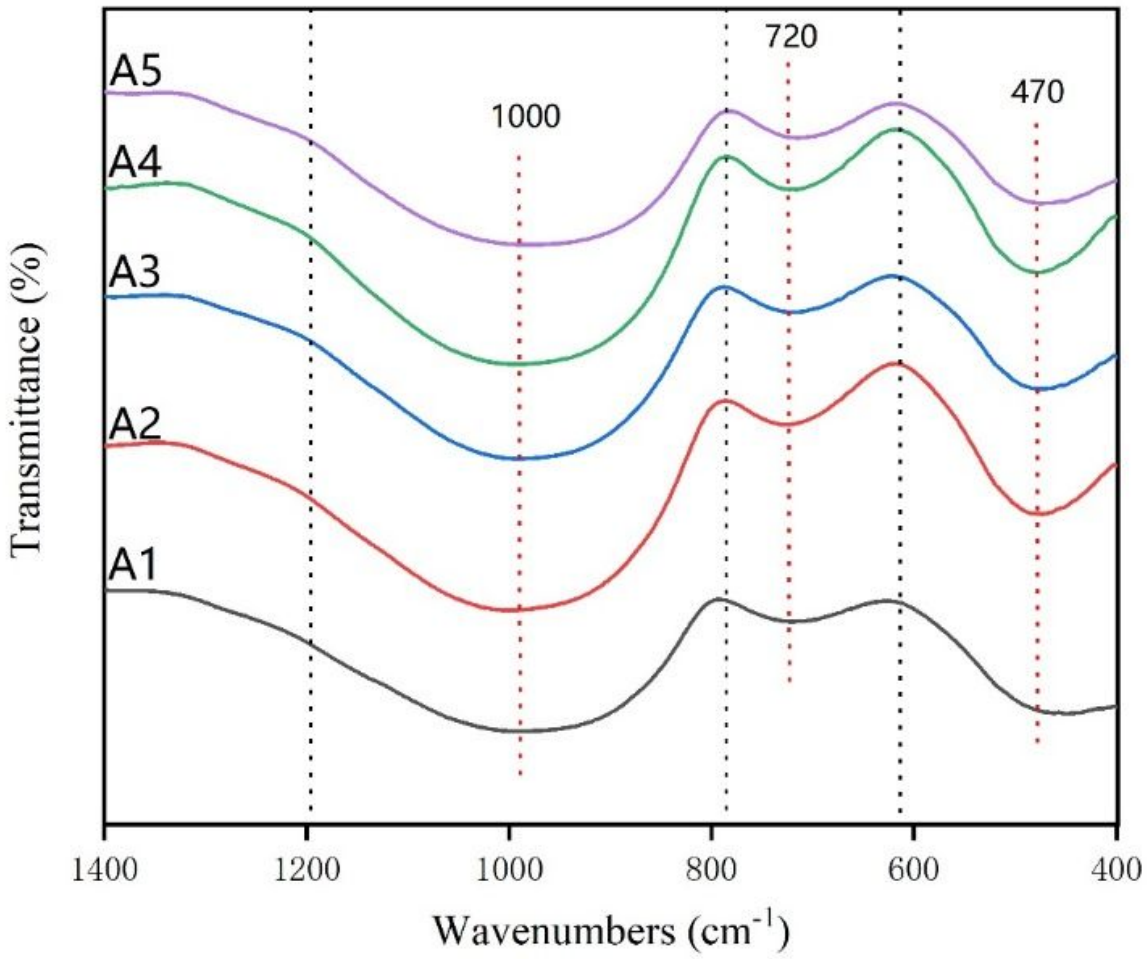


**Figure 4**

FTIR of glass with different Al2O3/SiO2.

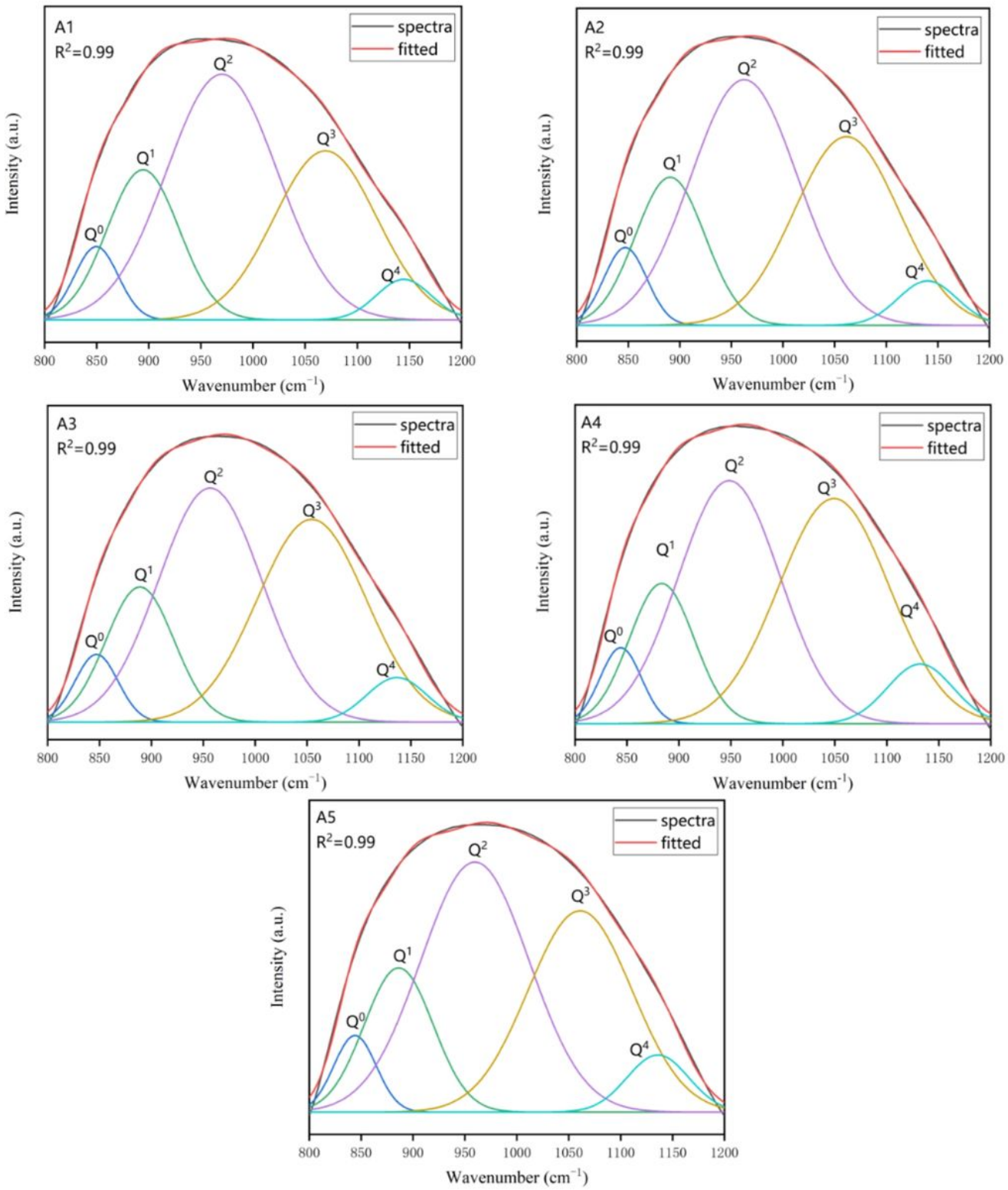


## Figure 5

Deconvoluted infrared spectra (800-1200 cm−1) of glasses with different Al2O3/SiO2.

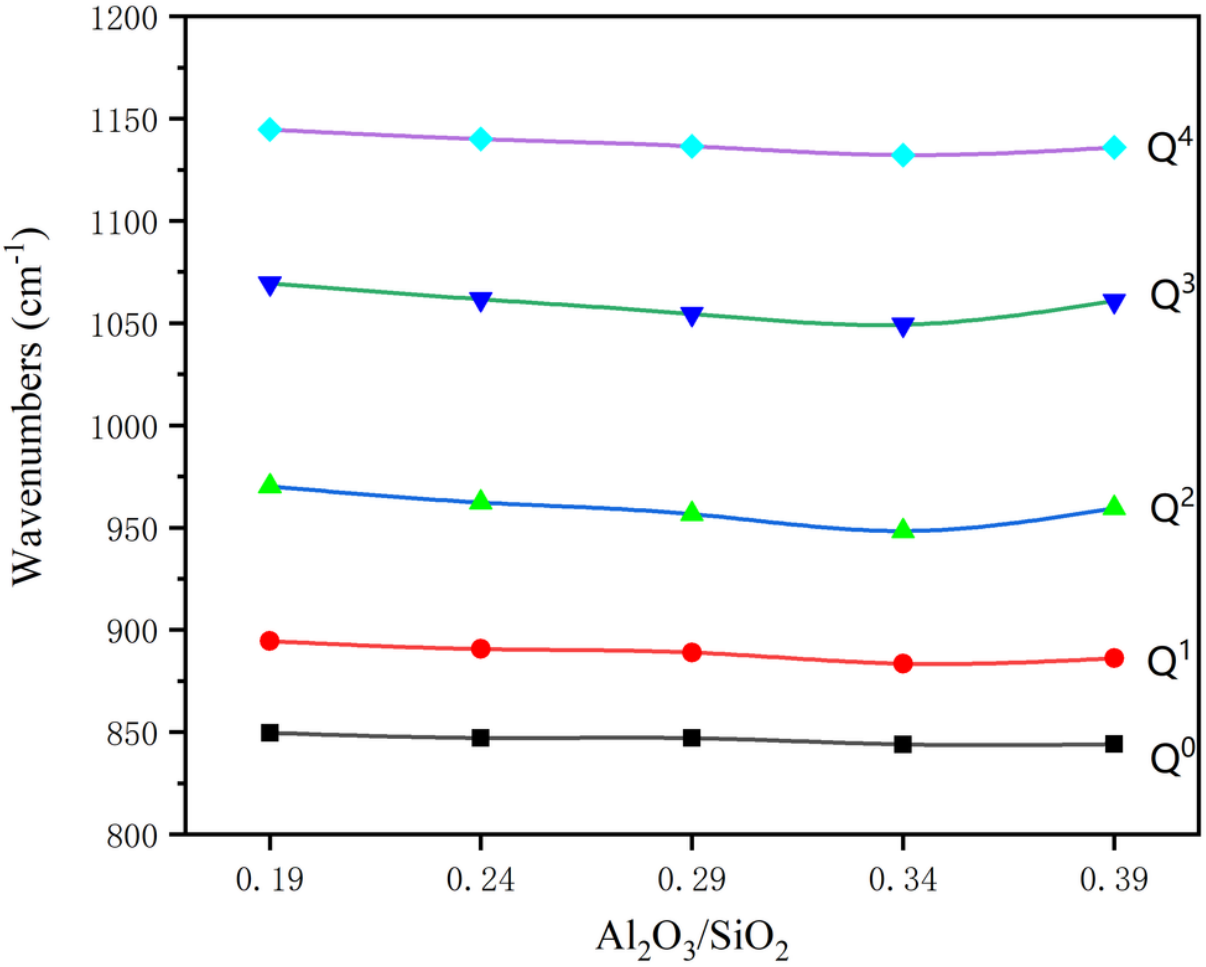


**Figure 6**

Variation distribution of peak position of Qn in glasses with different Al2O3/SiO2.

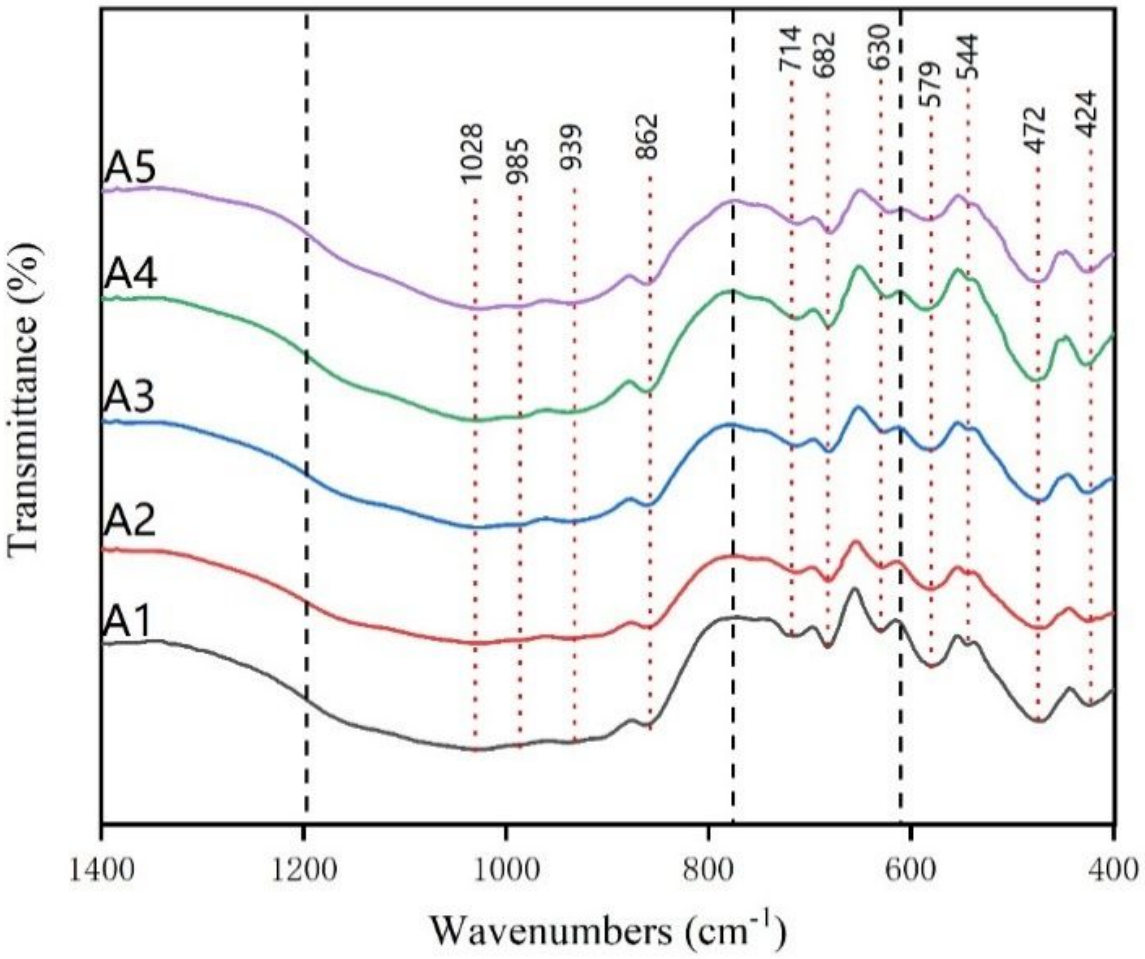


**Figure 7**

FTIR of glass-ceramics with different Al2O3/SiO2.

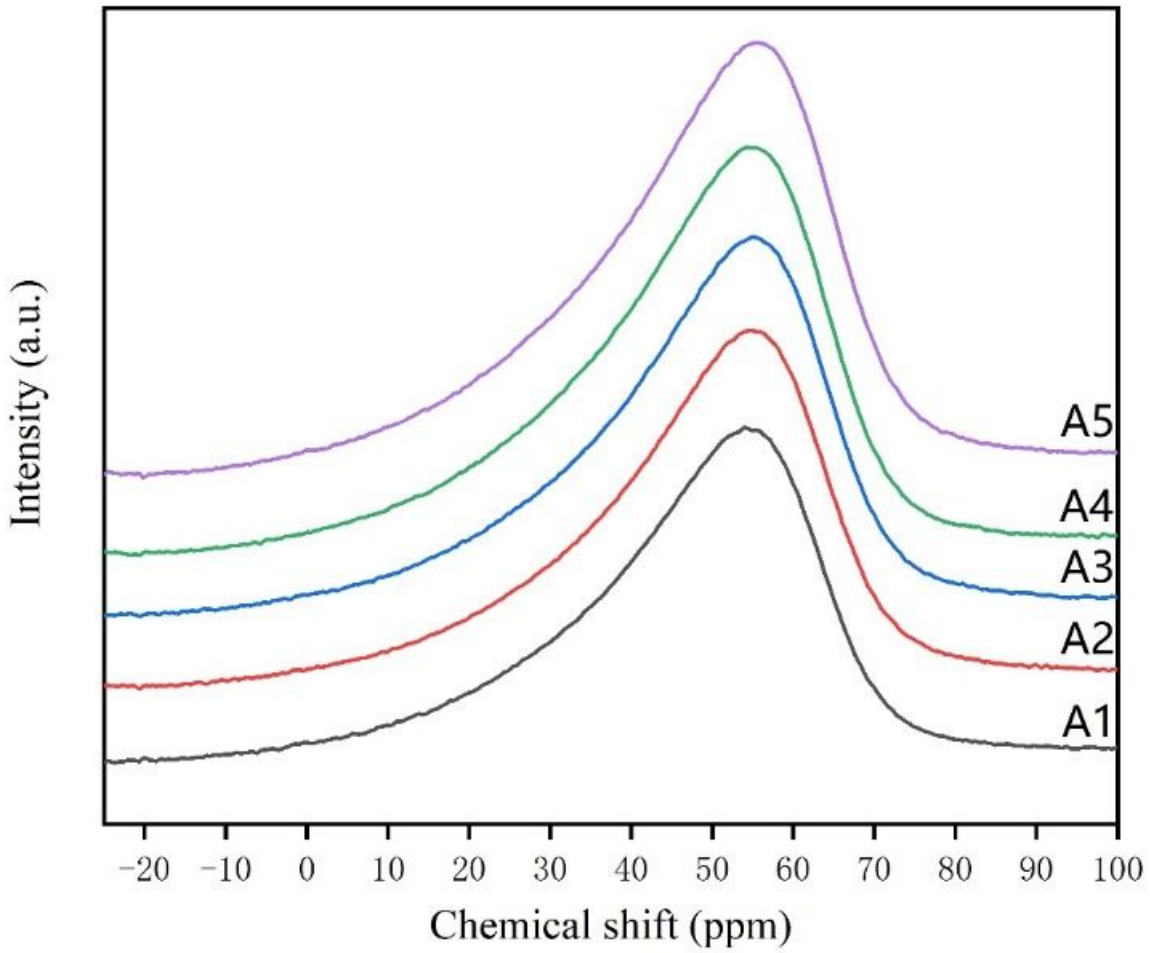


**Figure 8**

27Al NMR spectra of the glasses with different Al2O3/SiO2.

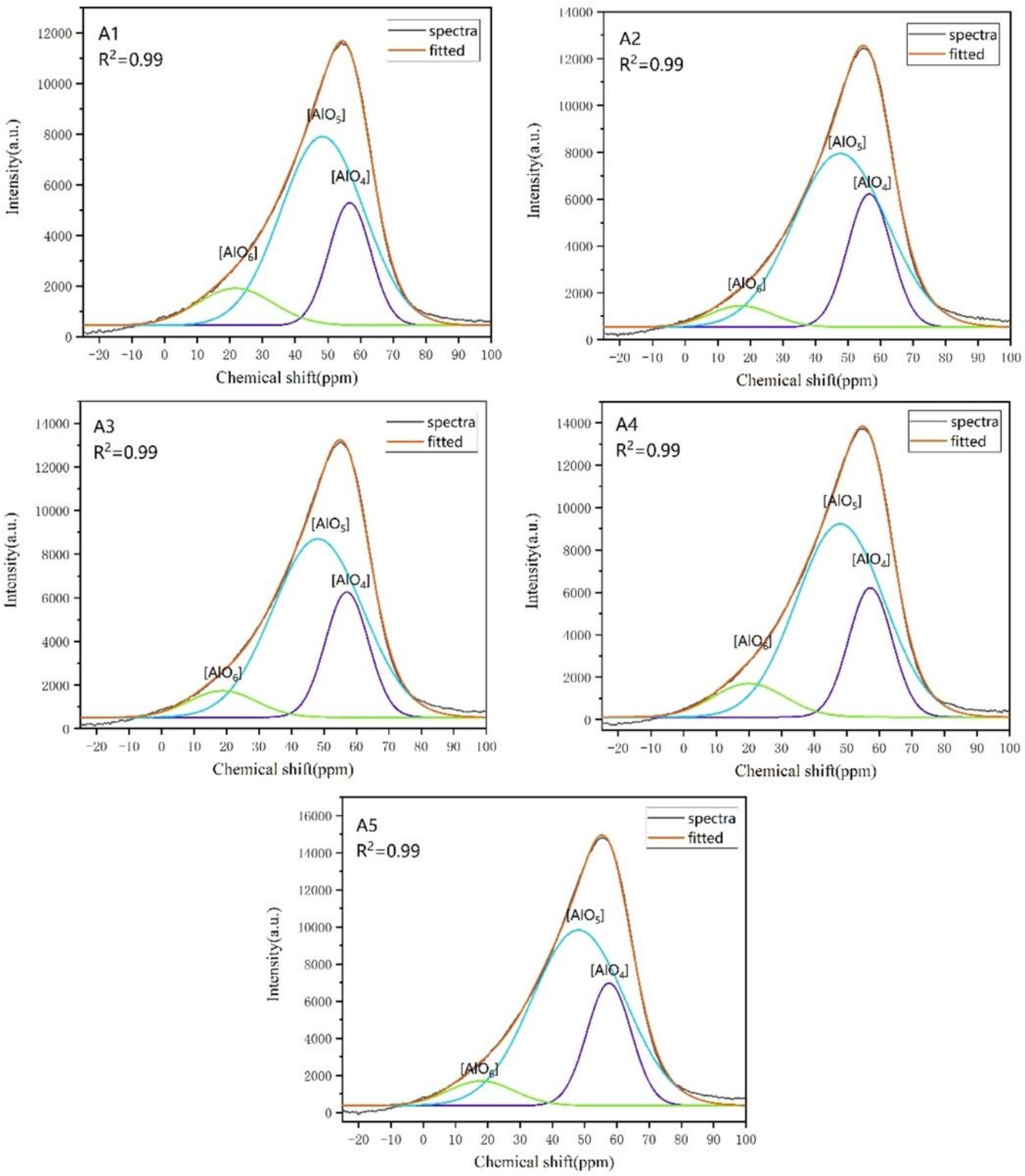


## Figure 9

Deconvolution of the 27Al NMR spectra for glasses with different Al2O3/SiO2.

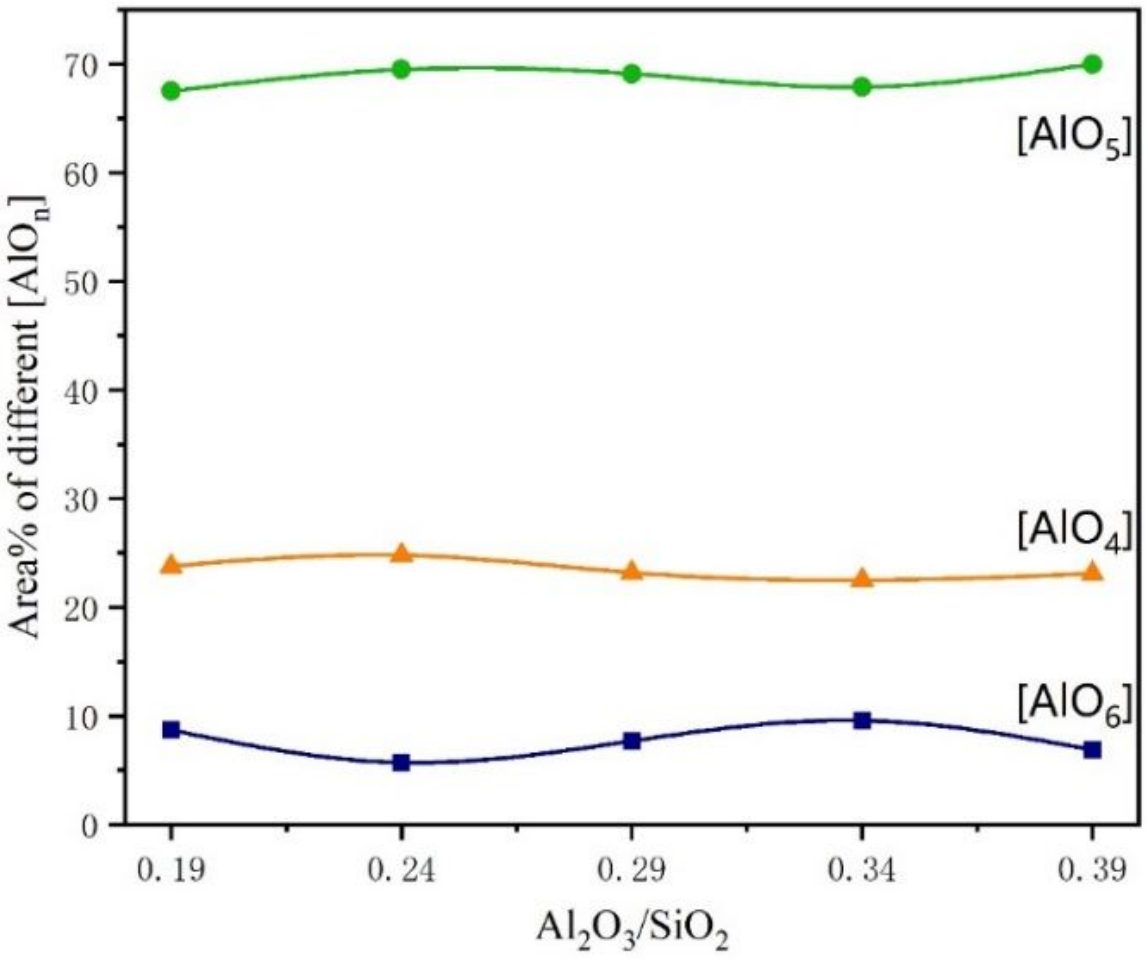


**Figure 10**

Area % of different [AlOn] in patent glasses with different Al2O3/SiO2; n=4, 5, 6.

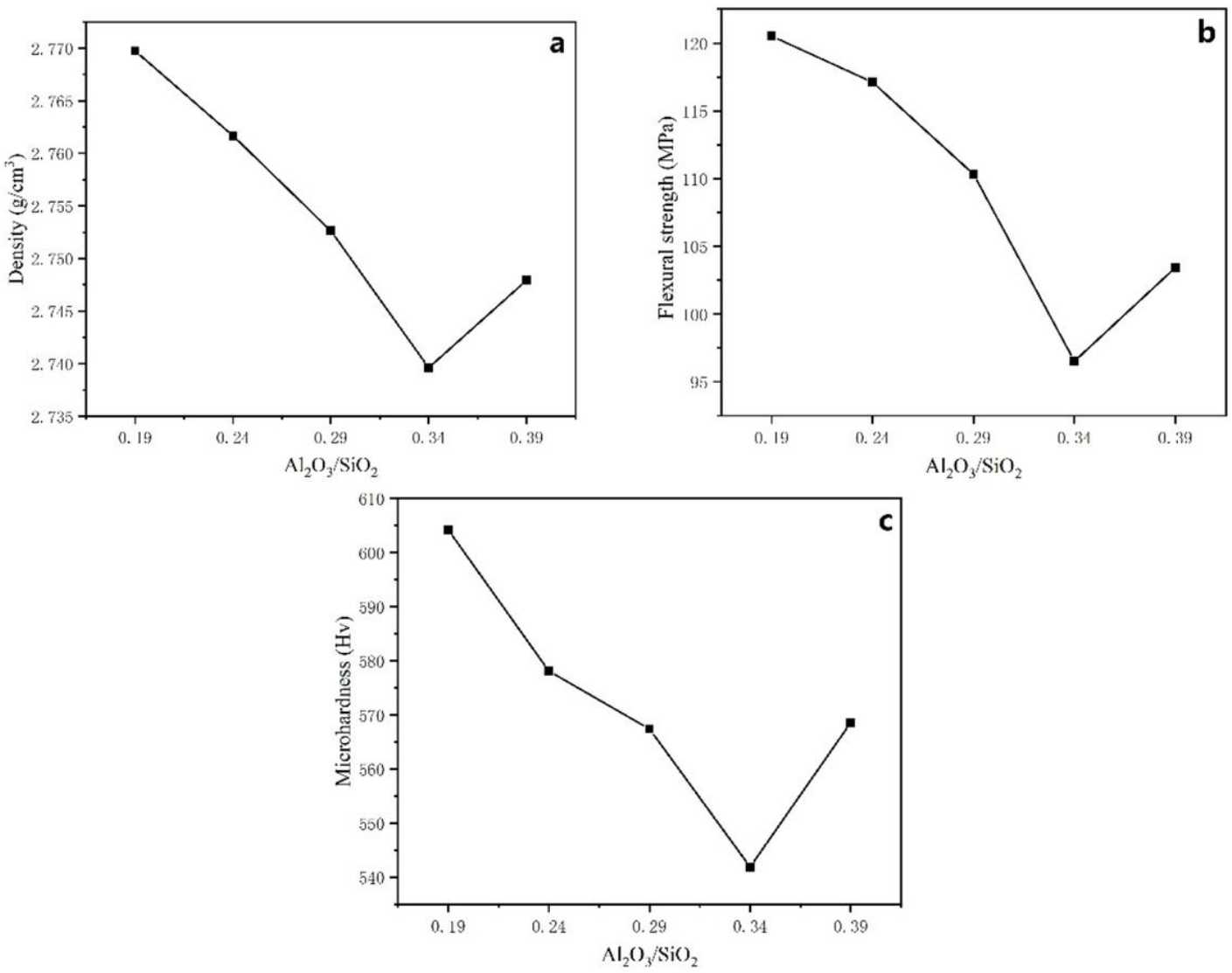


## Figure 11

Physical and mechanical properties of glass-ceramics with different Al2O3/SiO2 (a: volume density of glass-ceramics; b: bending strength of glass-ceramics; c: microhardness of glass-ceramics).